Monthly Notices of the ROYAL ASTRONOMICAL SOCIETY

MNRAS **503,** 336–343 (2021) doi:10.1093/mnras/stab416
Advance Access publication 2021 February 12

Dust entrainment in galactic winds

R. Kannan [1]★ M. Vogelsberger [2] F. Marinacci [3] L. V. Sales [4] P. Torrey [5] and L. Hernquist [1]

[1] *Center for Astrophysics | Harvard & Smithsonian, 60 Garden Street, Cambridge, MA 02138, USA*
[2] *Kavli Institute for Astrophysics and Space Research, Massachusetts Institute of Technology, Cambridge, MA 02139, USA*
[3] *Department of Physics & Astronomy 'Augusto Righi', University of Bologna, via Gobetti 93/2, I-40129 Bologna, Italy*
[4] *Department of Physics & Astronomy, University of California, Riverside, 900 University Avenue, Riverside, CA 92521, USA*
[5] *Department of Astronomy, University of Florida, 211 Bryant Space Sciences Center, Gainesville, FL 32611, USA*

Accepted 2021 February 9. Received 2021 February 6; in original form 2020 November 10

ABSTRACT

Winds driven by stellar feedback are an essential part of the galactic ecosystem and are the main mechanism through which low-mass galaxies regulate their star formation. These winds are generally observed to be multiphase with detections of entrained neutral and molecular gas. They are also thought to enrich the circumgalactic medium around galaxies with metals and dust. This ejected dust encodes information about the integrated star formation and outflow history of the galaxy. Therefore it is important to understand how much dust is entrained and driven out of the disc by galactic winds. Here, we demonstrate that stellar feedback is efficient in driving dust-enriched winds and eject enough material to account for the amount of extraplanar dust observed in nearby galaxies. The amount of ejected dust depends on the sites from where they are launched, with dustier galaxies launching more dust-enriched outflows. Moreover, the outflowing cold and dense gas is significantly more dust enriched than the volume filling hot and tenuous material. These results provide an important new insight into the dynamics, structure, and composition of galactic winds and their role in determining the dust content of the extragalactic gas in galaxies.

Key words: radiative transfer – dust, extinction – ISM: general – galaxies: ISM.

1 INTRODUCTION

Extraplanar dust is typically observed in emission in the far-infrared (FIR) and sub-mm frequencies, which are sensitive to cool dust (Hughes, Gear & Robson 1990; Radovich, Kahanpää & Lemke 2001; Roussel et al. 2010; Meléndez et al. 2015; McCormick et al. 2018). It is also observed in the form of highly structured absorbing clouds against the background stellar light (Howk & Savage 2000). Starlight is also scattered by the dust, forming reflection nebulae (RN) which are detected in the ultraviolet (UV) bands (Hoopes et al. 2005; Hodges-Kluck & Bregman 2014; Seon et al. 2014; Hodges-Kluck et al. 2016). These observations have shown that the dust and warm ionized gas occupy separate regions of space, representing distinct phases of the multiphase extraplanar gas. The volume filling factor of the material traced by extraplanar dust is also much smaller than that of the ionized gas (Howk & Savage 2000; Rossa et al. 2004). Moreover, in the starbursting galaxy M82, the outflow velocity of dust is substantially lower than that of both ionized and molecular gas (Yoshida, Kawabata & Ohyama 2011; Yoshida et al. 2019), indicating that dust grains in the wind are kinematically decoupled from the gas. These observations indicate that the dynamics of dusty outflows is complex. Galactic scale winds in low-mass haloes ($M_{\rm halo} \lesssim 10^{12}\,{\rm M}_{\odot}$) are believed to be mainly launched by the energy injection of supernova (SN) explosions in the interstellar medium (ISM; Chevalier & Clegg 1985; Strickland et al. 2000). These winds are capable of entraining cold molecular and neutral gas (Heckman & Thompson 2017; Naab & Ostriker 2017) and might also be able to sweep up dust and expel them into the CGM of galaxies. Dust grains might also reform by accretion of metals after the shocked outflowing wind has cooled below the dust sputtering temperature (Richings & Faucher-Giguère 2018a, b). Radiation pressure by the continuum absorption and scattering of photons on dust grains is another mechanism that has been invoked to explain large-scale galactic winds in highly luminous starbursting galaxies and in high-luminosity quasars (Murray, Quataert & Thompson 2005; Barnes et al. 2018).

Modelling the physics and dynamics of these dusty winds is paramount to understand the complex interplay of star formation, feedback, gas outflows, and inflows that regulate the formation and evolution of galaxies. There has been a lot of effort into modelling galactic winds. Most current galaxy formation models are quite empirical with the efficiency and dynamics of the winds designed to reproduce the large-scale properties of galaxies (see for e.g. Vogelsberger et al. 2014, 2020). These models launch hydrodynamically decoupled winds that lack the ability to model low-temperature gas or dust implying that they are unable to accurately capture the structure of the wind. While novel models have been implemented in these simulations, to track the dust distribution in the ISM (McKinnon et al. 2017; Li, Narayanan & Davé 2019), the artificial wind launching mechanisms imply that the mass loading of and the dust entrainment properties in the wind are set by the input parameters and are therefore, not self-consistent predictions of the simulation. Recently, Aoyama et al. (2018) and Aoyama, Hirashita & Nagamine (2020) used a sophisticated dust model that can follow the grain-size distribution of dust to model the extinction curves of

★ E-mail: rahul.kannan@cfa.harvard.edu

Milky Way like galaxies. However, they did not address how the dust is entrained in galactic winds.

In this paper, we present high-resolution simulations of isolated galaxies that self-consistently account for dust production and destruction mechanisms such as enrichment by SN and asymptotic giant branch (AGB) stars, metal deposition on to dust grains, destruction in supernova remnants, thermal sputtering, and dust-radiation coupling. We investigate the ability of stellar feedback driven winds in transporting dust from the ISM to the outer parts of the galactic halo. Our methodology is introduced in Section 2, the main results are presented in Section 3 and finally, our conclusions are given in Section 4.

2 SIMULATIONS

The simulations are performed with AREPO-RT (Kannan et al. 2019) a novel radiation hydrodynamic (RHD) extension of the moving mesh hydrodynamic code AREPO (Springel 2010). The reduced speed of light approximation with $\tilde{c} = 10^3$ km s^{-1} is used in order to reduce the computational time.

Gas is allowed to cool down to 10 K, with the cooling function split in into four separate terms, (i) primordial cooling from hydrogen and helium ($\Lambda_{\rm p}$), (ii) metal cooling ($\Lambda_{\rm M}$), (iii) photoelectric heating ($\Lambda_{\rm PE}$), and (iv) cooling due to dust–gas-radiation field ($\Lambda_{\rm D}$) interactions (see Kannan et al. 2020b, for more details). Star formation and feedback closely follows the implementation of the SMUGGLE model (Marinacci et al. 2019; Kannan et al. 2020b). Briefly, cold gas above a density threshold $n_{\rm th} = 10^3$ cm^{-3}, is converted in star particles using the standard probabilistic approach. Three feedback mechanisms related to young stars, radiative feedback, stellar winds from young O, B, and AGB stars and finally SN feedback are implemented. Photoheating, radiation pressure, and photoelectric heating are modelled self-consistently through the radiative transfer scheme, which discretizes the radiation filed into six frequency bins, infrared (IR; 0.1−1.0 eV), Optical (1.0−5.6 eV), far ultraviolet (FUV; 5.6−11.2 eV), Lyman Werner (LW: 11.2−13.6 eV), hydrogen ionizing (13.6−24.6 eV), He I ionizing (24.6−54.4 eV), and He II ionizing (54.4−∞ eV) photons. Stellar winds from two classes of stars, massive, short-lived OB ($\lesssim$8 M$_\odot$) stars and AGB stars are included. SN is modelled using a boosted momentum injection method that compensates for the cooling losses that occur due to the inability to resolve the Sedov–Taylor phase. The discrete nature of SN explosions is also modelled by imposing a time-step constraint for each stellar particle based on its age (i.e. evolutionary stage), such that the expectation value for the number of SN events per time-step is of the order of unity.

The simulations employ a novel self-consistent dust formation and destruction model (McKinnon et al. 2017) that tracks the mass of dust in five chemical species (C, O, Mg, Si, and Fe) for each individual gas cell. It accounts for three distinct dust production channels namely, SN II, SNIa and AGB stars (Dwek 1998). The dust is assumed to be dynamically coupled to the gas and is passively advected along with the gas when the hydrodynamic equations are solved.

The mass of dust in the ISM will increase due to the gas-phase elements colliding with existing grains (Dwek 1998) and decrease due to shocks from SN remnants (McKee 1989) and sputtering in high temperature gas (Tsai & Mathews 1995). These three process together control the dust mass of the cell

$$\frac{{\rm d}M_{\rm dust}}{{\rm d}t} = \left(1 - \frac{M_{\rm dust}}{M_{\rm metal}}\right)\left(\frac{M_{\rm dust}}{\tau_{\rm g}}\right) - \frac{M_{\rm dust}}{\tau_{\rm d}} - \frac{3\,M_{\rm dust}}{\tau_{\rm sp}}\,, \tag{1}$$

where $M_{\rm dust}$ and $M_{\rm metal}$ are the total mass of dust and metals in the cell, and $\tau_{\rm g}$ is the characteristic growth time-scale, which depends on both the temperature and density of gas (Yozin & Bekki 2014)

$$\tau_{\rm g} = \tau_{\rm g}^{\rm ref}\left(\frac{\rho^{\rm ref}}{\rho}\right)\sqrt{\frac{T^{\rm ref}}{T}}\,, \tag{2}$$

where $\tau_{\rm g}^{\rm ref} = 200$ Myr, is an overall normalization influenced by factors like atom-grain collision sticking efficiency and grain cross-section, $\rho^{\rm ref}$ and $T^{\rm ref}$ are the reference density and temperature set to 1 H atom cm^{-3} and 20 K, respectively. $\tau_{\rm d}$ is the dust destruction time-scale due to SN shocks and is given by

$$\tau_{\rm d} = \frac{m_{\rm gas}}{\beta\zeta\,M_{\rm s}(100)}\,, \tag{3}$$

where $m_{\rm gas}$ is the mass of the gas cell, $\beta = 0.3$ is the efficiency with which grains are destroyed in SN shocks, ζ is the local Type II SN rate calculated self-consistently for all gas particles experiencing an SN event and $M_{\rm s}(100) = 6800\,{\rm M}_\odot$ is the mass of gas shocked to at least 100 km s^{-1}. Finally, $\tau_{\rm sp}$ is given by (Tsai & Mathews 1995)

$$\tau_{\rm sp} = (0.17\ {\rm Gyr})\left(\frac{a}{0.1\,\mu{\rm m}}\right)\left(\frac{10^{-27}\ {\rm g\ cm^{-3}}}{\rho}\right)\left[\left(\frac{T_0}{T}\right)^{\omega} + 1\right], \tag{4}$$

where $T_0 = 2 \times 10^6$ K is the temperature above which the sputtering rate is constant and $\omega = 2.5$ controls the sputtering rate at low temperatures.

We run two high resolution isolated simulations of a MW like galaxy (MW; $M_{\rm halo} = 1.53 \times 10^{12}\,{\rm M}_\odot$) and a Large Magellanic Cloud-like galaxy (LMC; $M_{\rm halo} = 1.09 \times 10^{11}\,{\rm M}_\odot$). We set up an equilibrium galaxy model consisting of a dark matter halo, a bulge and a stellar and gaseous discs in a domain of size $L_{\rm box}$. The DM halo and the bulge are modelled with a Hernquist profile (Hernquist 1990; Springel, Di Matteo & Hernquist 2005). The gas and the stellar disc have an exponential profile in the radial direction with an effective radius $r_{\rm g}$ and $r_{\rm d}$, respectively. The vertical profile of the stellar disc follows a sech^2 functional form with the scaleheight h. The vertical profile of the gaseous disc is computed self-consistently to ensure hydrostatic equilibrium at the beginning of the simulation. The initial gas temperature is set to 10^4 K. The gas in the disc has a metallicity equal to a value of $Z_{\rm init}$. The lack of cosmological gas inflow into the disc can generate unrealistic gas metallicities. To avoid this, the material returned from stars to the ISM has the same chemical composition of the star particle (i.e. production of new heavy elements is turned off). In this way, the initial metallicity $Z_{\rm init}$ does not increase with time.[1] The dark matter halo is modelled as a static background gravitational field, that is not impacted by the baryonic physics. The structural parameters of the galaxies under consideration are given in Table 1. Each galaxy setup is run with a stellar mass resolution of $2.8 \times 10^3\,{\rm M}_\odot$ and gas mass resolution of $1.4 \times 10^3\,{\rm M}_\odot$. The corresponding gravitational softening lengths are $\epsilon_\star = 7.1$ and $\epsilon_{\rm gas} = 3.6$ pc, respectively.

3 RESULTS

Fig. 1 presents a visualization generated from the IR (red component), optical (yellow component) and the ionizing radiation (blue component) emission from the disc in the MW (top panel), and LMC (bottom panel) simulations as seen edge on. These visualizations

[1]This also means that the feedback driven winds generated in the simulations expand into a very low density medium, while in realistic situations they will interact in a complex manner with the gas in the CGM. Understanding how the properties of dusty winds are altered by the CGM is beyond the scope of this work and will be investigated in future works.

Table 1. The structural parameters of the MW and LMC like galaxies simulated in this work. From left to right, the columns list the name of the simulation, the total halo mass, virial velocity, concentration parameter, mass of the bulge, mass of the disc, scale radius of the stellar disc, scale height of the stellar disc, scale radius of the gas disc, gas fraction in the disc, the initial metallicity of the stars and gas, and the computational box size.

Galaxy	$M_{\rm halo}$ ($M_\odot$)	v_{200} (km s^{-1})	c	$M_{\rm bulge}$ ($M_\odot$)	$M_{\rm disc}$ ($M_\odot$)	$r_{\rm d}$ (kpc)	h (pc)	$r_{\rm g}$ (kpc)	$f_{\rm gas}$	$Z_{\rm init}$ ($Z_\odot$)	$L_{\rm box}$ (kpc)
MW	1.53×10^{12}	169	12	1.5×10^{10}	4.74×10^{10}	3.0	300	6.0	0.16	1.0	875
LMC	1.09×10^{11}	70	14	1.8×10^{8}	2.3×10^{9}	1.4	140	2.8	0.19	0.5	285

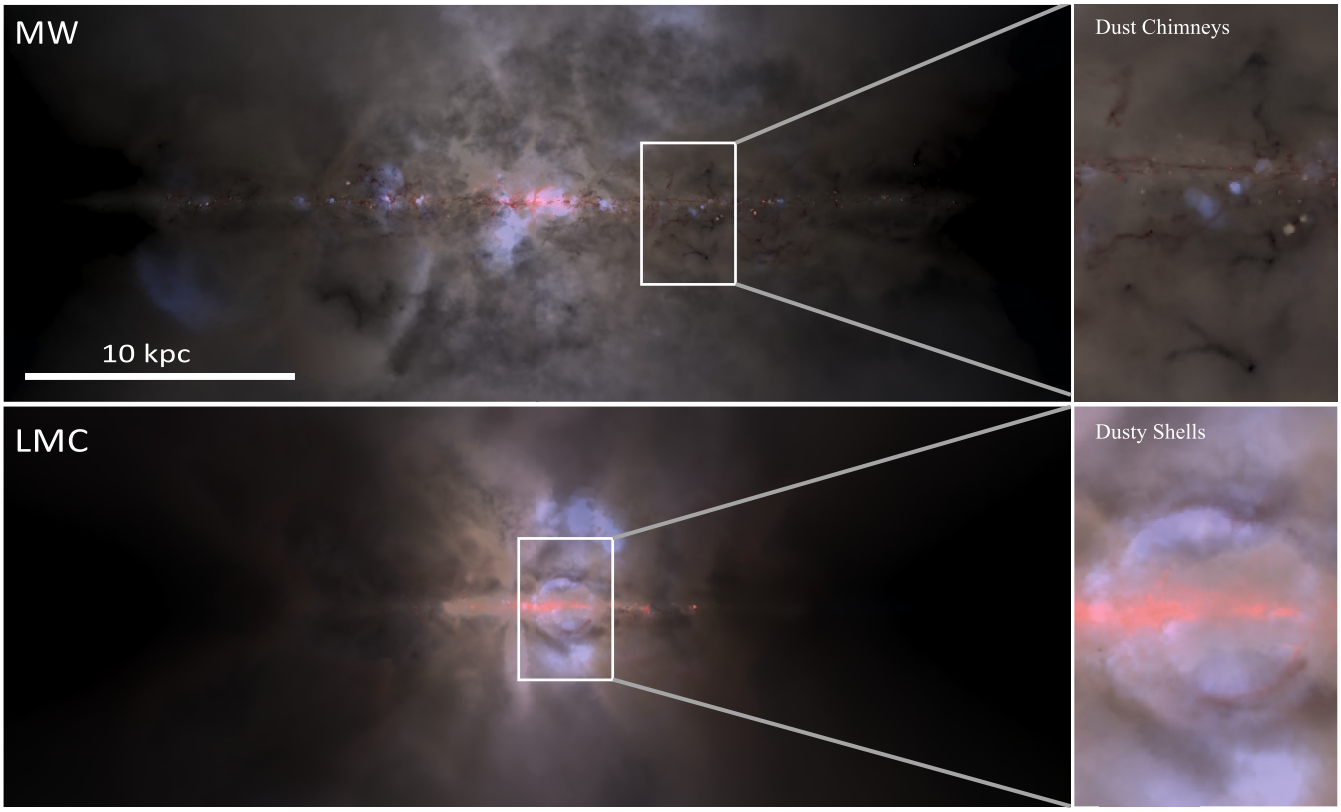

Figure 1. A visualization generated from the IR (red component), optical (yellow component) and the ionizing radiation (blue component) emission from the disc in the MW (top panel), and LMC (bottom panel) simulations as seen edge on. Dusty outflows and expanding dusty shells and chimneys are visible in both simulations. The insets show magnified examples of these topological features. These features are a clear sign of stellar feedback driven dusty outflows in galaxies (Howk & Savage 2000).

demonstrate the manifold dusty extraplanar gas, extending above and below the disc. A variety of complex dust topologies can be observed including expanding, IR bright, dusty shells, around UV bright regions and a rich complex of filaments, and chimney-like features (see magnified insets) that extends up to ∼2−3 kpc above and below the plane of the galaxy. Such features have also been observed in nearby galaxies and have been attributed to hydrodynamical outflows driven by star formation activity in the disc (Howk & Savage 1999, 2000).

A quantitative picture of the wind is obtained by measuring the gas mass (solid curves) and dust mass loading (dashed curves) factors (η), defined as the ratio of the mass outflow rate to the star formation rate of the galaxy, as a function of simulation time (see left-hand panel of Fig. 2). These quantities are measured at a height of 2 kpc from the plane of the disc. The gas mass loading factor hovers at ∼2 for the MW (red curves) and at ∼15 for the LMC run (blue curves) throughout the duration of the simulation. This is in agreement with previous rough theoretical estimates (Muratov et al. 2015). On the other hand, the loading factor of the dust predicted by the model is lower by about a factor of 200−500. These low dust loading factors are mainly due to the fact that the dust-to-gas ratio of the disc, from where these outflows are launched, is usually less than 1 per cent. This is demonstrated more clearly in the right-hand panel of Fig. 2, which shows the dust-to-gas ratio (D) of the wind (calculated as the mass loading of dust divided by the mass loading of gas; solid curves) compared to the dust-to-gas ratio of the central disc (within two times the stellar half-mass radius; dashed curves). D of the MW disc is about a factor of 2 higher than the disc in the LMC simulation. This is because, the metallicity of the gas in the MW simulation is initialized to the canonical solar abundance value ($Z_\odot$) while the metallicity of the LMC run is $Z_\odot/2$, in order to match the observational estimates (Madden et al. 2013). Although the simulations are initialized without dust, the gas of the disc is enriched during the course of the simulation, such that the average D is ∼0.01 and ∼4×10^{-3} for the MW and LMC discs, respectively, which is in excellent agreement with observational estimates (Roman-Duval et al. 2014; Giannetti et al. 2017). The figure shows that the exact

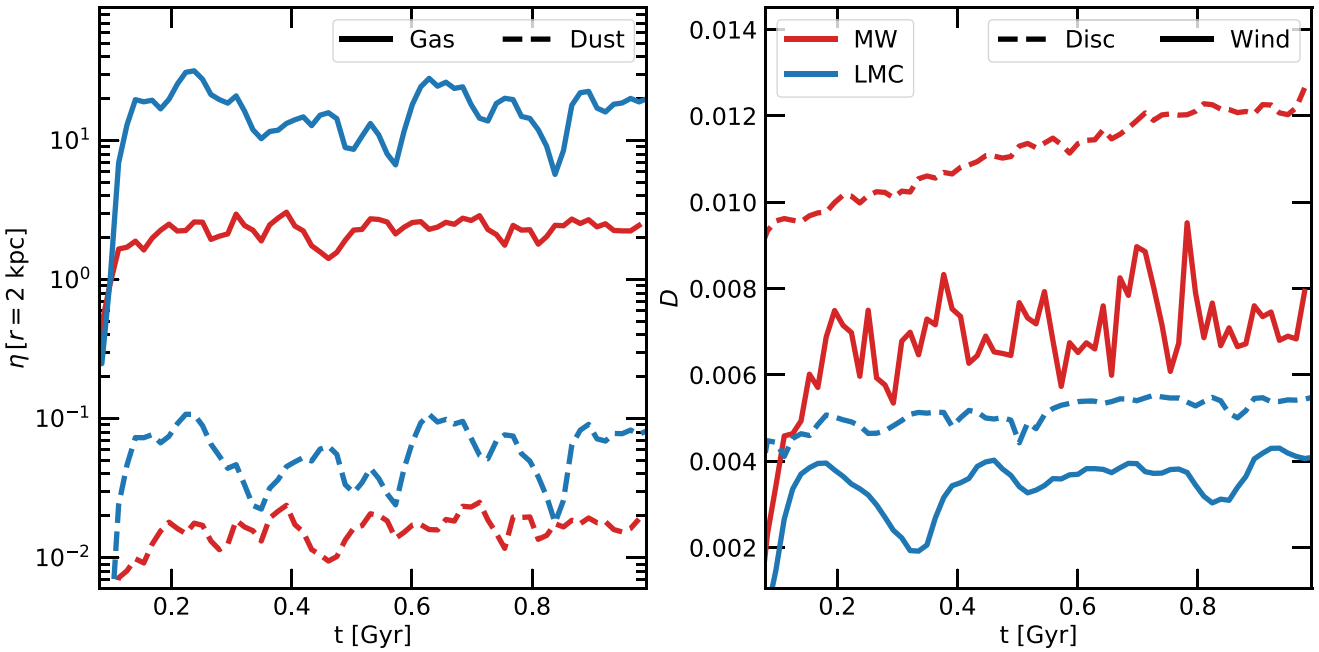

Figure 2. The left-hand panel shows the gas mass (solid curves) and dust mass (dashed curves) loading factors as a function of the simulation time in the MW (red curves) and LMC simulations (blue curves). The gas mass loading factor hovers at ∼2 for the MW simulation (red curves) and at ∼15 for the LMC simulation (blue curves) throughout the duration of the simulation in agreement with previous rough theoretical estimates (Muratov et al. 2015). The right-hand panel shows the dust-to-gas ratio (D) of the outflow (solid curves) and the disc (dashed curves) as a function of simulation time for both the simulations. The mass loading factor of dust predicted by the model is lower by about a factor of 200−500. The plot also shows that the dustier galactic disc is able to launch more dust-enriched outflows.

level of dust enrichment in outflows depends on the dust abundance in the disc from which the winds are launched, with the dustier disc launching more enriched winds. The fraction of dust in the disc is always higher than in the outflow, by about 30–40 per cent, meaning that the outflows are less dust enriched than the sites from which they are launched. This is due to the fact that a certain fraction of the dust is destroyed in SN shocks and thermal sputtering in the high-temperature gas resulting from SN explosions. We note that turning off the radiation pressure does not change the mass loading factors of either the dust or the gas in both the MW and LMC simulations. This is because the star formation rates of these galaxies are moderately low (MW: $\sim 2\,M_\odot\,yr^{-1}$; LMC: $\sim 0.1\,M_\odot\,yr^{-1}$), such that the light-to-mass ratio is not large enough to launch winds via radiation pressure.[2] This is consistent with results of previous theoretical consideration (Sales et al. 2014; Rosdahl et al. 2015; Kannan et al. 2020a) that showed that radiation pressure is only important in dense, compact, and rapidly star-forming galaxies like the M82 (Thompson et al. 2015; Zhang et al. 2018). These results demonstrate that dust is efficiently expelled out of the disc by SN-driven outflows, offering a path to explain the transport of dust from galaxies into the circumgalactic medium.

A thorough understanding of the gas and dust structure in the wind is obtained by plotting a 2D of the relative dust-to-gas ratio ($D_{\rm wind}/D_{\rm disc}$) as a function of the gas temperature and density (Fig. 3) in the MW (left-hand panel) and LMC (right-hand panel) simulations.[3] We consider all outflowing gas that is at a height between 2 and 10 kpc, both above and below the disc mid-plane. Interestingly, both the MW and LMC simulations show a complex wind structure with the density and temperature ranging from $10^{-6} \lesssim n_{\rm H}\,[{\rm cm}^{-3}] \lesssim 1$ and $1000 \lesssim T\,[{\rm K}] \lesssim 10^7$, respectively. The amount of dust entrained in the wind shows a strong dependence on its temperature. In the MW simulation, the relative dust-to-gas-ratio ($D_{\rm wind}/D_{\rm disc}$) decreases gradually from a value of about 0.9 for gas with temperatures less than 8000 K, to less than 0.3 in the hot gas phase ($T > 5 \times 10^5$ [K]). Interestingly, the LMC simulation shows less variation with the relative D decreasing to only ∼0.6 even in the hot phase. This is because the initial D of the LMC disc is only $\sim 4 \times 10^{-3}$ (compared to $D \sim 10^{-2}$ for the MW run) and since the dust destruction mechanism is proportional to the initial mass of dust in the gas cell (see equation 1), the destruction rate will be lower. Therefore, while dust-to-gas ratio of the wind in both simulations is similar, the normalization factor ($D_{\rm disc}$) is smaller in the LMC simulation leading to less variation in the relative dust-to-gas ratio. On the other hand, almost all the density dependence of D arises from the fact that the cold gas needs to be necessarily dense in order to self-shield from the local radiation background.

The hot wind is generated from the interiors of SN remnants that break out from the disc of the galaxy and expands adiabatically into the halo generating a large-scale galactic wind. This gas has, therefore, been depleted of dust due to the shocks from SN remnants (McKee 1989) and thermal sputtering, causing D of the hot wind to

[2]This is only true under the assumption that the gas and dust are fully dynamically coupled. If the dust and gas are only weakly coupled then radiation pressure might be able to induce a drift velocity between the dust and gas fluids, increasing the dust loading factor (Draine 2011; McKinnon et al. 2019).

[3]We note that a single average value of $D_{\rm disc}$ calculated within two times the stellar half-mass radius is used for this plot. This is representative of the sites from which the winds are launched because most of the star formation in these simulations takes place within this central region.

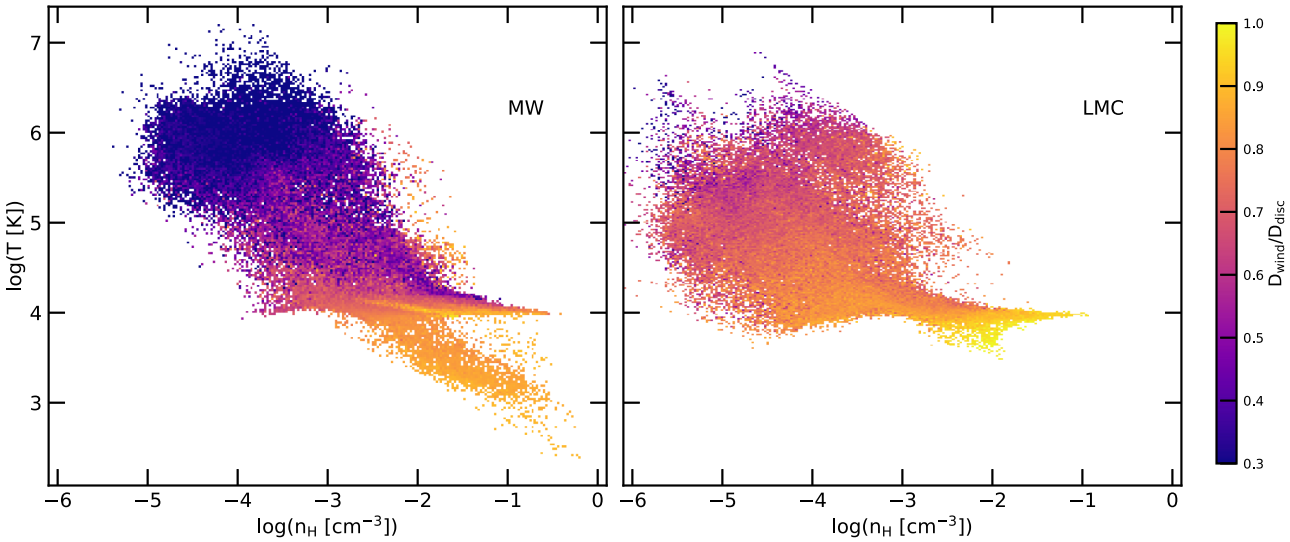

Figure 3. A 2D histogram showing the relative dust-to-gas ratio ($D_{outflow}/D_{disc}$) of the wind material ($2 \leq z\,(\mathrm{kpc}) < 10$) as a function of the density and temperature for the MW (left-hand panel) and LMC (right-hand panel) simulations.

be much lower than D of the disc. This low D combined with the fact that the hot wind has a low-mass loading factor ($\eta_{hot} \sim 0.3$) means that the amount of dust carried out by this phase is quite small ($\lesssim 10$ per cent). Most of the ejected dust is entrained in the warm phase (defined as any outflowing material with $T \leq 5 \times 10^5$ K) of the wind (Fig. 4). These warm clouds are accelerated by expanding superbubbles pushing on the surrounding ISM. The typical ejection velocity is quite low (80–100 km s^{-1} at the disc scaleheight) and is insufficient to escape the gravitational potential of the galaxy. It follows an almost ballistic path, reaching heights of $\gtrsim$ 2–5 kpc,[4] before falling back on to the disc. The warm phase is, therefore, not a true galactic-scale wind but a small-scale fountain flow that alternates between inflow and outflow dominated phases. The hot phase, on the other hand is a true wind with very little gas and dust falling back on to the disc The ballistic behaviour indicates that warm clouds are not significantly accelerated by ram pressure of the hot, high-velocity gas that is flowing out around them. Rather, they are primarily accelerated via direct energy and momentum input from SNe, close to the disc mid-plane (Kim & Ostriker 2018; Kannan et al. 2020a). This warm material, unaffected by shocks, is more suitable for dust grains to survive, allowing for it to be almost as dust enriched as the disc it has been launched from. We are, therefore, able to reproduce a realistic outflow, that is multiphase, with the dense warm fountain flow being more dust enriched than the volume filling, large-scale hot wind (Rossa et al. 2004; Hodges-Kluck et al. 2016).

Finally, Fig. 5, shows the amount of dust mass ejected out of the disc of the galaxy ($2 \leq z\,(\mathrm{kpc}) < 10$) by the galactic wind, as a function of the stellar mass of the galaxy in the MW (filled red circle) and LMC (filled blue circle) simulations compared to the observational estimates for the nearby dwarf (McCormick et al. 2018) and spiral galaxies (Hodges-Kluck et al. 2016). The error bars show the time variation in the amount of dust after the disc in the simulation has settled down ($t > 0.2$ Gyr). Despite the fact that dust masses of the dwarf (emission in the FIR from *Herschel*) and spiral (reflected UV light of dust grains with *GALEX* and *Swift*) galaxies are obtained using very different techniques, they do show a relatively tight correlation with the stellar mass of the galaxy.

The amount of extraplanar dust in the MW and LMC galaxies are about $\sim 3 \times 10^6$ and $\sim 3 \times 10^5$ M$_\odot$, respectively, which is in agreement with the observational estimates. We note that the total amount of dust mass ejected (above 2 kpc but not above 10 kpc) from the disc of the galaxy integrated over the entire duration of the simulation time (1 Gyr; unfilled circles) is about a factor of $\sim$10 higher than current mass of the extraplanar dust found in the galaxies. This is because most of the dust ejected by the galaxies falls back down as part of the fountain flow and only a small fraction of it remains outside the disc of the galaxy at any given point in time. This implies that the amount of extraplanar dust depends chiefly on the current/recent star formation rate of the galaxy and the corresponding small-scale fountain flow set up by it, and should therefore be largely independent of the cosmological environment of the galaxy. Higher mass galaxies generally have higher star formation rates, which leads to larger outflow rates. They also contain dustier discs, which launch more dust-enriched outflows. These two factors combine to generate a positive stellar mass correlation with the extraplanar dust mass of the galaxy.

4 CONCLUSIONS

We have presented high resolution isolated simulations of a MW like and a LMC like galaxies with detailed modelling of the dynamics of dust formation, evolution, and destruction. Using these simulations, we investigate the level of dust entrainment in stellar feedback driven winds. Our main results are summarized as follows.

(i) The gas mass loading factor for the MW and LMC simulations is about $\sim$2 and $\sim$15, respectively, in agreement with previous estimates. On the other hand, we predict that the dust mass loading factor should be lower by about 200–500.

(ii) The exact level of dust enrichment in the winds depends on the dust content of the disc from where they are launched with the dustier gas disc launching more dust-enriched outflows.

[4]The exact height reached by the fountain flow will depend on the ratio between the initial kinetic energy received and the gravitational potential of the galaxy.

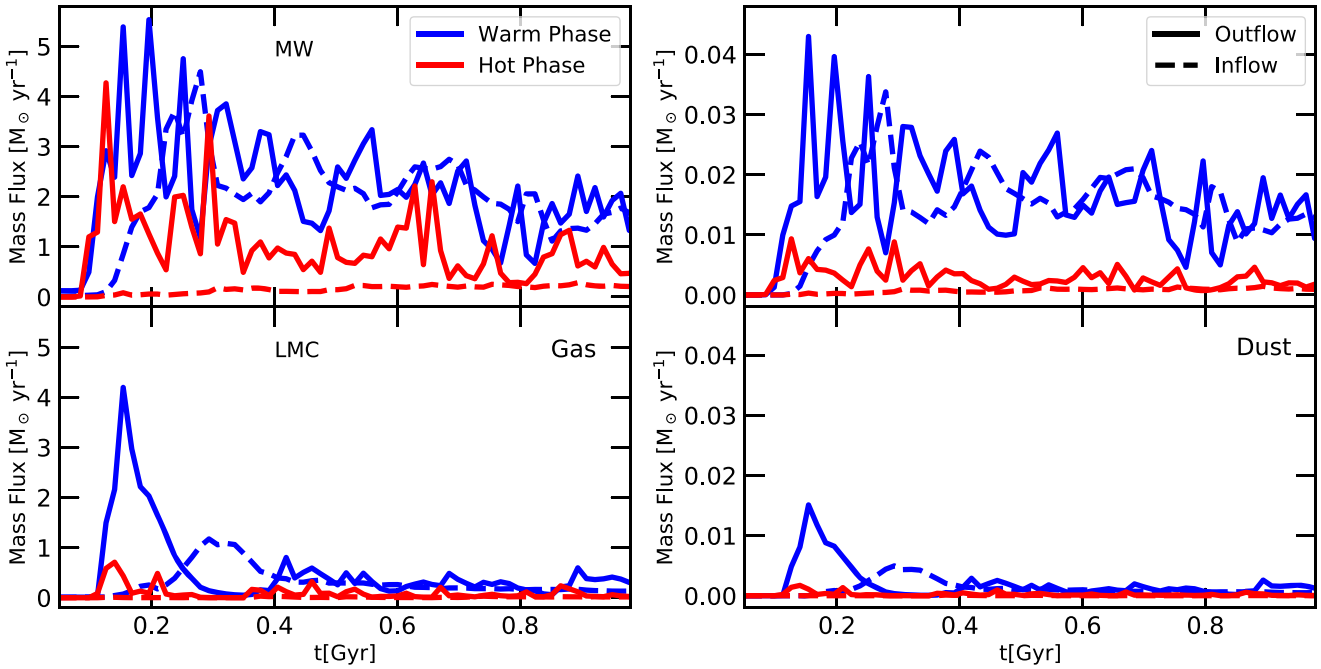

Figure 4. The gas (left-hand panels) and dust (right-hand panels) inflow (dashed curves) and outflow (solid curves) rates for the warm (blue curves) and hot (red curves) gas phases as a function of simulation time at a height of 2 kpc from the disc in the MW (top panel) and LMC (bottom panel) simulations. The warm gas and the dust entrained in it alternates between outflow and and inflow phases with very little of it escaping the potential of the galaxy. The hot wind on the other hand is dust depleted and is mostly outflowing, with very little gas falling back on to the disc.

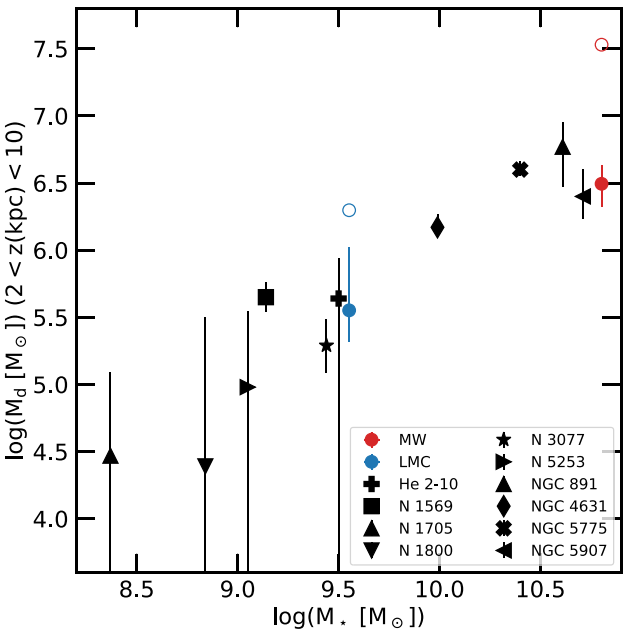

Figure 5. The total amount of extraplanar dust mass ($2 \leq z\,(\mathrm{kpc}) < 10$) as a function of the total stellar mass of the galaxy in the MW (red point) and LMC (blue point) simulations. For comparison, we also show the observational estimates from nearby dwarf (McCormick et al. 2018, N1705, N1800, N5253, N1569, He2-10, N3077) and spiral (Hodges-Kluck et al. 2016, NGC 891, NGC 4631, NGC 5775, NGC 5907) galaxies. The corresponding unfilled circles show the total amount of dust mass ejected from the disc during the entire duration of the simulation time (1 Gyr), which is about an order of magnitude larger than the current amount of extraplanar dust in the galaxy.

(iii) The D of the warm gas (which is cycling as a galactic fountain flow, back and forth between the disc and the halo) is only slightly lower than D of the disc it is launched from, while D of the hot wind is lower by about a factor of 3. This is because, the hot gas is primarily ejected from the sites of SN explosions, which are efficient at destroying dust due to the shocks from SN remnants. The warm gas on, the other hand, is accelerated by expanding superbubbles pushing on the surrounding ISM, and is therefore, unaffected by shocks, making it suitable for dust grains to survive.

(iv) Galactic winds launch enough material to completely account for the amount of extraplanar dust observed in nearby dwarf and spiral galaxies. Most of the ejected dust participates in a small-scale fountain flow and only a small fraction of it remains outside the plane of the disc at any given point.

We can therefore conclude that stellar feedback driven outflows expel enough dust from the disc of the galaxies to explain the amount of extraplanar dust in galaxies observed in the nearby Universe. Our results are only slightly dependent on the resolution, with a lower resolution simulation showing winds that are only about ~ 20 per cent less dust enriched (see Appendix A for more details). We note that this process is only efficient in transporting dust to within a few kpc from the Galactic Centre. In order to populate the outer parts of the galactic halo with dust, additional mechanisms to accelerate the cold gas, like ram pressure acceleration by the hot wind (Veilleux, Cecil & Bland-Hawthorn 2005) (purely hydrodynamical ram pressure acceleration has been shown to be an inefficient acceleration mechanism (Zhang et al. 2017) but additional physical processes such as magnetic fields (McCourt et al. 2015) and thermal conduction (Armillotta et al. 2017) might help the cold clouds to survive longer, increasing the effectiveness of this process), mixing of momentum from the hot to the cool phase (Schneider et al. 2020), radiation pressure from starlight (Thompson et al. 2015), acceleration

due to cosmic ray pressure (Simpson et al. 2016) or cooling of the hot gas at large radii (Thompson et al. 2016) might be required. In the future, we plan to extend this study to a fully cosmological framework which will allow us comprehensively quantify the dust content in the circumgalactic and intergalactic gas in the Universe. These findings will be especially important for current and upcoming sub-mm, FIR, and UV facilities like *Herschel*, *ALMA*, and *JWST* that will help to detect dusty winds (Hodges-Kluck et al. 2019) in a variety of galaxies at various redshifts.

DATA AVAILABILTIY

Raw data was generated by performing simulations at the NASA Pleiades computer. Derived data supporting the findings of this study are available from the corresponding author R.K. on request.

ACKNOWLEDGEMENTS

FM is supported by the Program 'Rita Levi Montalcini' of the Italian MIUR. LVS is thankful for the financial support from NASA through *HST*-AR-14582. Computing resources supporting this work were provided by the NASA High-End Computing (HEC) Program through the NASA Advanced Supercomputing (NAS) Division at Ames Research Center.

REFERENCES

Aoyama S., Hou K.-C., Hirashita H., Nagamine K., Shimizu I., 2018, MNRAS, 478, 4905
Aoyama S., Hirashita H., Nagamine K., 2020, MNRAS, 491, 3844
Armillotta L., Fraternali F., Werk J. K., Prochaska J. X., Marinacci F., 2017, MNRAS, 470, 114
Barnes D. J., Kannan R., Vogelsberger M., Marinacci F., 2020, MNRAS, 494, 1143
Chevalier R. A., Clegg A. W., 1985, Nature, 317, 44
Draine B. T., 2011, ApJ, 732, 100
Dwek E., 1998, ApJ, 501, 643
Giannetti A. et al., 2017, A&A, 606, L12
Heckman T. M., Thompson T. A., 2017, preprint (arXiv:1701.09062)
Hernquist L., 1990, ApJ, 356, 359
Hodges-Kluck E., Bregman J. N., 2014, ApJ, 789, 131
Hodges-Kluck E., Cafmeyer J., Bregman J. N., 2016, ApJ, 833, 58
Hodges-Kluck E., Corrales L., Veilleux S., Bregman J., Li J., Melendez M., 2019, BAAS, 51, 249
Hoopes C. G. et al., 2005, ApJ, 619, L99
Howk J. C., Savage B. D., 1999, AJ, 117, 2077
Howk J. C., Savage B. D., 2000, AJ, 119, 644
Hughes D. H., Gear W. K., Robson E. I., 1990, MNRAS, 244, 759
Kannan R., Vogelsberger M., Marinacci F., McKinnon R., Pakmor R., Springel V., 2019, MNRAS, 485, 117
Kannan R., Marinacci F., Simpson C. M., Glover S. C. O., Hernquist L., 2020a, MNRAS, 491, 2088
Kannan R., Marinacci F., Vogelsberger M., Sales L. V., Torrey P., Springel V., Hernquist L., 2020b, MNRAS, 499, 5732
Kim C.-G., Ostriker E. C., 2018, ApJ, 853, 173
Li Q., Narayanan D., Davé R., 2019, MNRAS, 490, 1425
Madden S. C. et al., 2013, PASP, 125, 600
Marinacci F., Sales L. V., Vogelsberger M., Torrey P., Springel V., 2019, MNRAS, 489, 4233
McCormick A. et al., 2018, MNRAS, 477, 699
McCourt M., O'Leary R. M., Madigan A.-M., Quataert E., 2015, MNRAS, 449, 2
McKee C., 1989, in Allamandola L. J., Tielens A. G. G. M., eds, Proc. IAU Symp. 135, Interstellar Dust. Kluwer, Dordrecht, p. 431
McKinnon R., Torrey P., Vogelsberger M., Hayward C. C., Marinacci F., 2017, MNRAS, 468, 1505
McKinnon R., Kannan R., Vogelsberger M., O'Neil S., Torrey P., Li H., 2021, MNRAS, 502, 1344
Meléndez M. et al., 2015, ApJ, 804, 46
Muratov A. L., Kereš D., Faucher-Giguère C.-A., Hopkins P. F., Quataert E., Murray N., 2015, MNRAS, 454, 2691
Murray N., Quataert E., Thompson T. A., 2005, ApJ, 618, 569
Naab T., Ostriker J. P., 2017, ARA&A, 55, 59
Radovich M., Kahanpää J., Lemke D., 2001, A&A, 377, 73
Richings A. J., Faucher-Giguère C.-A., 2018a, MNRAS, 474, 3673
Richings A. J., Faucher-Giguère C.-A., 2018b, MNRAS, 478, 3100
Roman-Duval J. et al., 2014, ApJ, 797, 86
Rosdahl J., Schaye J., Teyssier R., Agertz O., 2015, MNRAS, 451, 34
Rossa J., Dettmar R.-J., Walterbos R. A. M., Norman C. A., 2004, AJ, 128, 674
Roussel H. et al., 2010, A&A, 518, L66
Sales L. V., Marinacci F., Springel V., Petkova M., 2014, MNRAS, 439, 2990
Schneider E. E., Ostriker E. C., Robertson B. E., Thompson T. A., 2020, ApJ, 895, 43
Seon K.-I., Witt A. N., Shinn J.-H., Kim I.-J., 2014, ApJ, 785, L18
, Simpson C. M., Pakmor R., Marinacci F., Pfrommer C., Springel V., Glover S. C. O., Clark P. C., Smith R. J., 2016, ApJ, 827, L29
Springel V., 2010, MNRAS, 401, 791
Springel V., Di Matteo T., Hernquist L., 2005, ApJ, 620, L79
Strickland D. K., Heckman T. M., Weaver K. A., Dahlem M., 2000, AJ, 120, 2965
Thompson T. A., Fabian A. C., Quataert E., Murray N., 2015, MNRAS, 449, 147
Thompson T. A., Quataert E., Zhang D., Weinberg D. H., 2016, MNRAS, 455, 1830
Tsai J. C., Mathews W. G., 1995, ApJ, 448, 84
Veilleux S., Cecil G., Bland-Hawthorn J., 2005, ARA&A, 43, 769
Vogelsberger M. et al., 2014, Nature, 509, 177
Vogelsberger M., Marinacci F., Torrey P., Puchwein E., 2020, Nat. Rev. Phys., 2, 42
Yoshida M., Kawabata K. S., Ohyama Y., 2011, PASJ, 63, 493
Yoshida M., Kawabata K. S., Ohyama Y., Itoh R., Hattori T., 2019, PASJ, 71, 87
Yozin C., Bekki K., 2014, MNRAS, 443, 522
Zhang D., Thompson T. A., Quataert E., Murray N., 2017, MNRAS, 468, 4801
Zhang D., Davis S. W., Jiang Y.-F., Stone J. M., 2018, ApJ, 854, 110

APPENDIX A: RESOLUTION DEPENDENCE

To test the effect of resolution, we re-simulate the MW galaxy at a lower resolution ('MW-LR'). This galaxy is run with a stellar mass resolution of 2.2×10^4 M$_\odot$ and gas mass resolution of 1.1×10^4 M$_\odot$. The corresponding gravitational softening lengths are $\epsilon_\star = 21.4$ and $\epsilon_{\rm gas} = 10.7$ pc, respectively. This corresponds to about a factor of 10 lower mass resolution and about 3 times lower spatial resolution. The structural parameters of the galaxy and the simulation model are the same. Fig. A1 shows D of the outflow divided by D of the disc as a function of simulation time in the MW (solid curve) and MW-LR (dashed curve) simulations. The results are relatively converged with the outflow in the MW-LR simulation only slightly less dust enriched ($<$ 20 per cent) than the higher resolution MW run for the entire duration of the simulation time. This then translates to about a factor of 2 decrease (Fig. A2) in the amount of extragalactic dust in the MW-LR (blue open point) simulation compared to the MW run (red filled point), which is well within the observational error bars. These plots show that our model is fairly robust with respect to resolution.

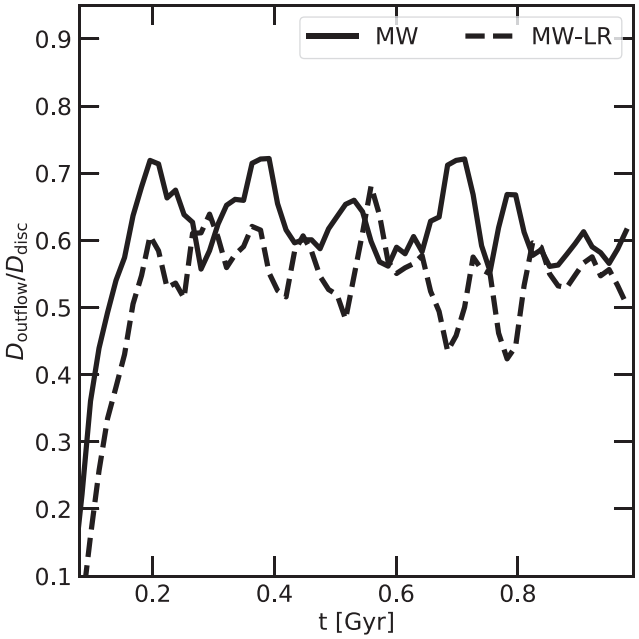

Figure A1. The dust-to-gas ratio (D) of the outflow divided by D of the disc as a function of simulation time in the MW (solid curve) and MW-LR (dashed curve) simulations.

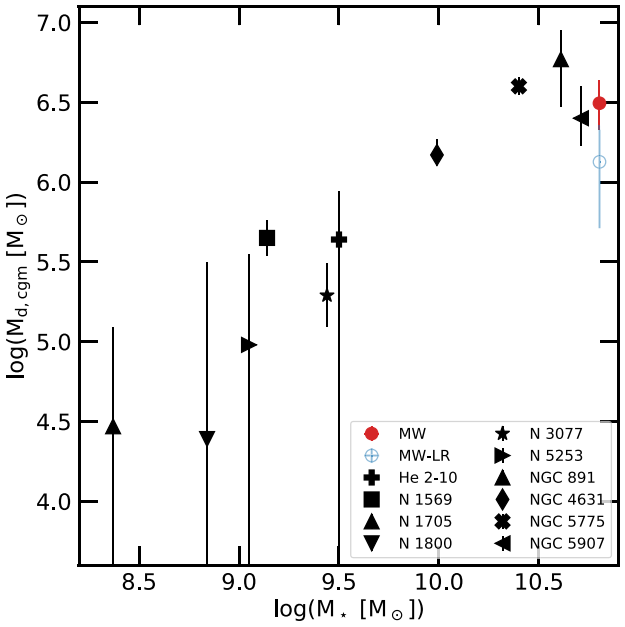

Figure A2. The total amount of extragalactic dust mass ($2 \leq z$ (kpc) < 10) as function of the total stellar mass of the galaxy in the MW (red filled point) and MW-LR (blue open point) simulations compared to observational estimates.

This paper has been typeset from a TEX/LATEX file prepared by the author.